First Analysis of Jupiter in Gamma Rays and a New Search for Dark Matter

Rebecca K. Leane[1, *] and Tim Linden[2, †]

[1] *SLAC National Accelerator Laboratory, Stanford University, Stanford, CA 94039, USA*
[2] *Stockholm University and The Oskar Klein Centre for Cosmoparticle Physics, Alba Nova, 10691 Stockholm, Sweden*

We present the first dedicated gamma-ray analysis of Jupiter, using 12 years of data from the *Fermi* Telescope. We find no robust evidence of gamma-ray emission, and set upper limits of $\sim 10^{-9}$ GeV cm^{-2} s^{-1} on the Jovian gamma-ray flux. We point out that Jupiter is an advantageous dark matter (DM) target due to its large surface area (compared to other solar system planets), and cool core temperature (compared to the Sun). These properties allow Jupiter to both capture and retain lighter DM, providing a complementary probe of sub-GeV DM. Our analysis focuses on the annihilation of sub-GeV DM to long-lived particles, which can escape the Jovian surface and decay into gamma rays. In this regime, we constrain DM-proton scattering cross-sections as low as 10^{-41} cm^2, which is up to ten orders of magnitude more sensitive than direct detection, and subject to fewer astrophysical uncertainties than other limits in this parameter space. Our work motivates follow-up studies with upcoming MeV telescopes such as AMEGO and e-ASTROGAM.

I. INTRODUCTION

KING of the Roman gods, Jupiter, commanded lightning, thunder, and storms. Analogous to the Greek god Zeus, he exerted his power with lightning bolts as weapons. Highlighting his stature, Jupiter was often portrayed ruling on a throne with a royal scepter in hand, ♃. His luminous wrath won him the name of one of the brightest objects in the sky, *Iovis Stella* (the star of Jupiter). Today, it is known as Jupiter, which is the heaviest and largest planet in our Solar System.

For the first time, we perform a dedicated search for Jupiter's lightning bolts (gamma rays) with the *Fermi* Gamma-Ray Space Telescope (see [1]). These gamma rays could potentially be produced through the active acceleration of cosmic rays in Jovian magnetic fields [2], through the passive interaction of galactic cosmic rays with Jupiter's atmosphere (similar to Solar models [3]), or from Dark Matter (DM) annihilation. Using 12 years of *Fermi* Large Area Telescope (LAT) gamma-ray data, we perform a novel analysis that has been optimized for studies of solar system objects, such as the Sun [4, 5].

Over most of this energy range, we find no statistically significant evidence for gamma-ray emission, with a maximum local significance of 1.47σ for a power-law spectrum of $E^{-2.1}$. However, in the lowest-energy bins (<15 MeV), we find 5σ evidence for a gamma-ray excess. This excess is non-trivial to verify, owing to significant systematic uncertainties at the very edge of the *Fermi*-LAT effective energy range. However, it does motivate follow-up observations with future MeV-scale telescopes [6, 7].

Detecting, or ruling out, Jovian gamma ray emission would have important implications for DM. DM in the Galactic halo can be captured by Jupiter if it scatters with Jovian matter, loses sufficient kinetic energy, and becomes gravitationally bound. Jupiter is an advantageous DM detector for several reasons. First, compared to the Sun, it has a much cooler core. This low core temperature means that less kinetic energy is transferred to the DM, making it easier to capture and retain dark matter after the initial scattering. While DM evaporation inhibits Solar DM limits below a few-GeV, studies of Jupiter can probe MeV-scale DM. Second, compared to other planets, Jupiter is heavier and has a larger radius. This means it can capture more DM, and consequently has a larger DM annihilation rate. Third, Jupiter is the closest gas giant to Earth, indicating it should have the largest flux from any DM signal.

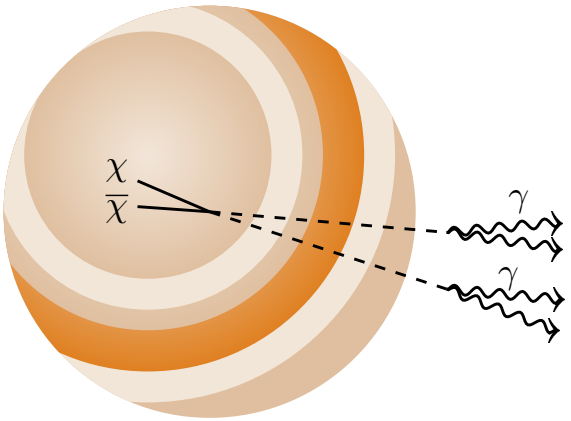

FIG. 1. Schematic of dark matter annihilation to long-lived particles in Jupiter. The long-lived particles can decay outside the Jovian surface, producing a new source of gamma rays.

While capture of DM in celestial objects has been considered in many objects, such as neutron stars and white dwarfs [8–47], the Sun [48–69], Earth [56, 70–72], Uranus [73, 74], Neptune and Jupiter [74, 75], Mars [72], and even exoplanets [76], detection prospects for DM signatures from Jupiter have not yet been studied. We will use our new gamma-ray search results to study observable DM signatures in Jupiter for the first time.

* Email: rleane@slac.stanford.edu; ORCID: 0000-0002-1287-8780
† Email: linden@fysik.su.se; ORCID: 0000-0001-9888-0971

Figure 1 illustrates the scenario we study; to detect DM annihilation inside Jupiter, the gamma rays must escape its atmosphere. Captured DM particles annihilate to long-lived mediators that subsequently decay outside of the Jovian surface, producing a new source of gamma rays that can be detected by the *Fermi* Telescope.

Long-lived particles are theoretically well-motivated [48, 77–81], and typically arise due to either small couplings (e.g., in the case of approximate symmetries), or light particle masses. Long-lived particles are currently extensively searched for in fixed-target and collider experiments [82–84], as well as astrophysical settings [47, 85–101]. Dark sectors with long-lived mediators have previously been considered in celestial bodies such as the Sun [48–69], Earth [56], and recently with large populations of brown dwarfs and neutron stars [47]. In this paper, we complement this existing parameter space. In fact, Jovian gamma-ray searches provide a MeV-scale cross-section sensitivity that significantly exceeds previous efforts. In light-mediator scenarios, are results are far superior to direct detection experiments.

This paper is organized as follows. In Section II, we detail our analysis of Jovian gamma rays with the *Fermi* Telescope, placing, for the first time, strong limits on the Jupiter gamma-ray flux. In Section III, we discuss DM capture and annihilation in Jupiter, and detail the long-lived mediator setup. We discuss constraints on the DM scattering cross section in Section IV. We conclude and discuss the implications of our results in Section V.

II. FERMI GAMMA-RAY DATA ANALYSIS

Here, we describe our data analysis framework and discuss our upper limits on the Jovian gamma-ray flux.

A. Data Analysis

We perform a novel *Fermi*-LAT analysis optimized for solar system objects that move with respect to the astrophysical background. Our analysis has previously been used to study solar gamma-ray emission (see Refs. [4, 5] for additional details). Here, we summarize the our analysis and note several choices tailored to studies of Jupiter.

The key to our method is the production of a fully *data-driven* background model. We first calculate the gamma-ray flux in a 45° region of interest (ROI) surrounding Jupiter. While this ROI vastly exceeds the ∼1° point-spread function (PSF) of *Fermi*-LAT photons at ∼1 GeV, such a large ROI is necessary to study Jupiter at energies near 10 MeV, where the 95% containment angle can approach 30°. We assign every gamma ray a "Jovian" coordinate by calculating its deviation in right ascension (RA) and declination (DEC) from the simultaneous Jupiter position. We then produce a background model by calculating the gamma-ray flux at each position in equatorial coordinates during periods when Jupiter was more than 45° away. Finally, we determine the equatorial exposure at every pixel in the Jovian coordinate system and subtract the background flux. This produces an "on"/"off" map that isolates Jupiter's flux and automatically accounts for astrophysical uncertainties that plague standard gamma-ray analyses.

1. *Dataset*

Our dataset includes all gamma rays with recorded energies between 10 MeV to 10 GeV and zenith angles below 90°. This significantly expands on previous studies that adopted a minimum energy of 100 MeV. Due to the large point-spread function and energy dispersion of *Fermi*-LAT events between 10–100 MeV, this adds significant modeling complexity, which we address below. We place standard instrumental cuts using `gtmktime`.

For each recorded gamma ray, we calculate its offset (in RA, DEC) from the simultaneous positions of Jupiter, the Sun and the Moon. We bin the data into 60 energy bins (20 logarithmically-spaced bins per decade), and calculate the exposure across the entire sky in 1 hr (3600-second) increments. Over this period, Jupiter moves only 0.003° with respect to the equatorial coordinate system, while the Sun moves ∼0.04 ° and the Moon moves 0.5°. These shifts are small compared to our ROIs and the instrumental PSF, justifying our treatment of each source as stationary *within* each time bin. For the exposure calculation, we utilize `phibins=10`. This is a non-standard choice which corrects for the fact that Jupiter's rotation through our solar system gives it a non-standard distribution in the instrumental coordinate ϕ, because the ϕ distribution is strongly biased by the solar position.

2. *Background Modeling*

To build our background model, we remove all photons recorded within 45° of Jupiter (our "on" region), within 40° of the Sun (which has an extended halo [102]), and within 20° of the Moon (which produces only disk emission). While the solar and lunar flux could be modeled and fit in the analysis (this approach was taken for lunar emission in Ref. [5]), this adds significant complexity because the Sun and Moon are much brighter than Jupiter. In this analysis, we simply mask these sources, losing only ∼15% of the total Jupiter exposure.

An important complication for studies of Jupiter (compared to solar analyses [5]), is the effect of flaring sources on the background model. Because the background model and source region are produced from photons recorded at different times, our model is sensitive to time-variable sources. In the solar analysis, this effect is significantly lessened for two reasons: (1) the Sun is bright, and its total luminosity in helioprojective coordinates dominates even the brightest flares, (2) the Sun moves through the equatorial coordinate system annu-

ally, and thus any variable source has been sampled (and averaged over) a dozen times. Jupiter, on the other hand, is a very dim gamma-ray source, which has an orbital period of 12 years, and thus has only moved through the equatorial coordinate system once.

To account for this effect, we also remove regions surrounding bright, variable background sources that lie near Jupiter. Utilizing the *Fermi* All-Sky Variability Analysis Catalog [103], we mask an ROI surrounding any source that ever approaches within 45° of Jupiter, and which has a peak-weekly flux (during any week, regardless of its proximity to Jupiter) exceeding 3×10^{-6} ph cm^{-2} s^{-1}. We remove a 5° ROI unless the source approaches to within 10° of Jupiter, in which case we remove a 10° ROI. We also remove a region around Geminga, which is not variable, but is extremely bright. Table I lists the ROIs removed from our analysis.

Source	R.A.	Dec.	ROI (°)
Sun	—	—	40
Moon	—	—	20
Crab	83.63	22.01	10
3C 279	194.05	-5.79	10
3C 273	187.28	2.05	10
PKS 1830-211	278.42	-21.06	10
3C 454.3	343.49	16.15	5
PKS 2247-131	342.50	-12.86	5
PKS 1329-049	203.02	-5.16	5
Geminga	98.48	17.77	5

TABLE I. Regions around bright sources that are removed from our analysis. These include sources that move with respect to the equatorial coordinate system (Sun, Moon), bright variable sources that enter the Jupiter ROI, and Geminga, which is not variable, but is very bright. Removing these ROIs decreases the exposure of Jupiter by ∼20%.

Using this background model we calculate the gamma-ray photon count at each RA/DEC during periods when Jupiter is not present. This is possible because Jupiter is far from any single RA/DEC most of the time. Because we have also calculated the exposure in equatorial coordinates in fine temporal bins, we can translate the photon count into a background gamma-ray flux. Finally, in every 3600-second window, we convert each point in equatorial coordinates to its simultaneous position in Jovian coordinates, producing an entirely data-driven background model at each point in Jovian coordinates.

Finally, we model Jupiter itself. Because the spatial extent of Jupiter is much smaller than the *Fermi* PSF at any energy, we treat Jupiter as a point-source, and utilize the tool *gtpsf* to calculate the effective PSF of Jupiter in each of our 60 energy bins and 3600-second time bins. We calculate the average PSF by performing a weighted average of each PSF over the simultaneous Jupiter exposure. While our background model automatically includes the effect of energy dispersion, we model the dispersion of Jupiter using the updated 15-parameter fit for P8R3 data described in Ref. [104].

Compared to standard analyses, our method has several advantages. Most importantly, all instrumental uncertainties (point-spread function, energy dispersion, effective area) are directly accounted for in the background model. This unlocks the power of our low-energy data, where these uncertainties become particularly acute.

3. *Likelihood Analysis*

We utilize `iminuit` to calculate the simultaneous fit of our background model and the Jupiter flux in each energy bin. In this case, we utilize a simple two-parameter fit, where the normalization of the Jupiter flux, and the normalization of the overall background template, are allowed to float independently in each energy bin. We note two important details. First, the normalization of the background template should equal 1, as the normalization of background sources should be independent of the position of Jupiter. Indeed, we find only very small deviations (on the order of $1-2\%$) from unity, verifying the accuracy of our techniques. Small errors may stem from variable sources, or instrumental exposure corrections that are correlated with the Jupiter position.

We allow the normalization of Jupiter to assume both positive or negative values. This is important, because constraining the Jupiter flux to be positive (and binning the data finely in energy) may make upward fluctuations appear overly significant. However, this choice can add complexity in the high-energy regime, because Poisson statistics are ill-defined when the total model expectation is negative in any pixel. Here, we follow Ref. [105], calculating the Poisson statistic from its absolute value in bins where the observed number of counts is 0, but ruling out negative fluctuations in bins where the number of observed photons is non-zero. This choice is numerically important, but has no practical impact on our results.

Figure 2 shows our model at energies between 1–3 GeV, including the gamma-ray flux within 45° of Jupiter, the gamma-ray flux predicted by our background model, and the resulting residual. Bright lines across the ROI correspond to bright sources moving through the Jovian coordinate system. The residuals are generally only a few percent, with maximum values near 20%. These primarily stem from flaring sources that we did not remove. We compare this result to an observation of Jupiter in the 1–3 GeV energy bin. The contribution from Jupiter will cover a much larger region in the lowest-energy bins, justifying our usage of a full 45° ROI.

Figure 3 shows the same four panels as in Fig. 2, but in the much lower energy range of 10–15 MeV. This lies at the extreme edge of the *Fermi*-LAT energy range, creating two significant effects. First, the effective area is very small, producing a small photon count and large statistical fluctuations. Second, the PSF is poor, with an 68% containment region of ∼15°. Despite these significant issues, our background model fits the data reasonably well. Notably the residual map appears consistent with Poisson fluctuations. Interestingly, we find several upward

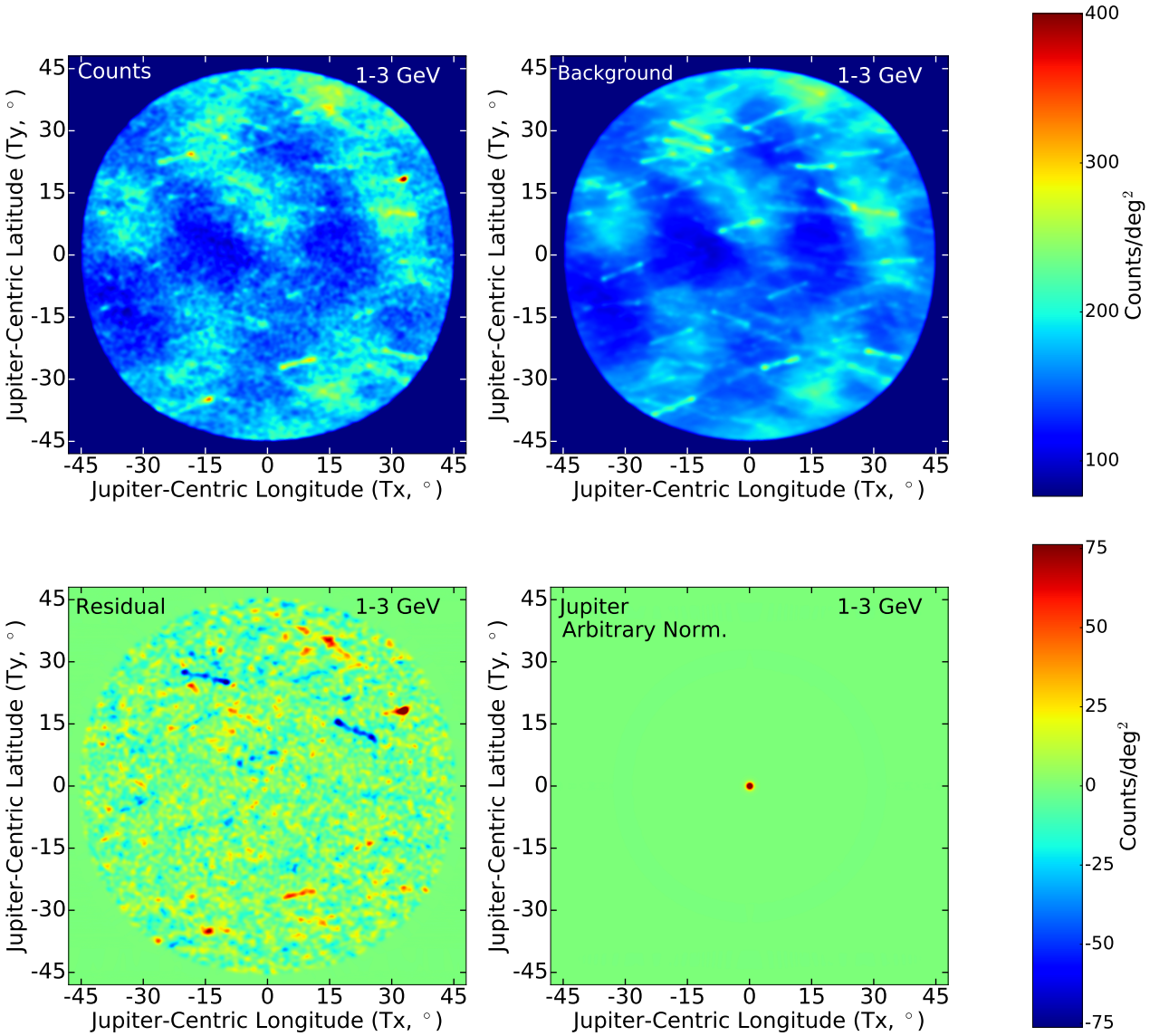

FIG. 2. *Fermi*-LAT gamma-ray data utilized in our analysis. For the visualization of this figure, we combine all energy bins between 1−3.16 GeV, and smear all results with a 1° Gaussian, choices that are not made in the analysis of our data. **Top Left:** Counts map produced by all events recorded within 45° of the position of Jupiter. **Top Right:** The background map, which is produced from observations of events calculated by examining identical regions in RA/DEC when Jupiter is not present. **Bottom Left:** The residual calculated by subtracting the model from our data. **Bottom Right:** An arbitrarily normalized morphology for Jupiter illustrating the scale of Jupiter (at relatively high energies) in our analysis.

fluctuations in the vicinity of Jupiter itself, and show in the next section that these residuals translate into a relatively significant excess consistent with Jovian emission.

B. Upper Limits on the Jovian Gamma-Ray Flux

Figure 4 shows the Jovian gamma-ray flux in our analysis. We note several important results. First, the overall flux of Jupiter is consistent with 0. For an E^{-2} gamma-ray spectrum we obtain a 95% confidence upper limit on the Jovian energy flux of 9.4×10^{-10} GeV cm^{-2} s^{-1} between 10 MeV – 10 GeV, while for a cosmic-ray motivated spectrum of $E^{-2.7}$ we obtain an upper limit of 3.2×10^{-9} cm^{-2} s^{-1}. For power-law spectra between $E^{-1.5}$ and $E^{-3.0}$, the significance of Jovian emission never exceeds 1.47σ.

Second, we note that the error bars in our analysis are highly correlated. This is due to the significant energy-dispersion of low-energy *Fermi*-LAT data, which smears the true Jovian energy flux between multiple energy bins. This effect decreases, from ∼30–50% in the lowest energy bins, to near 15% at GeV energies.

Third, we note that there is a statistically significant

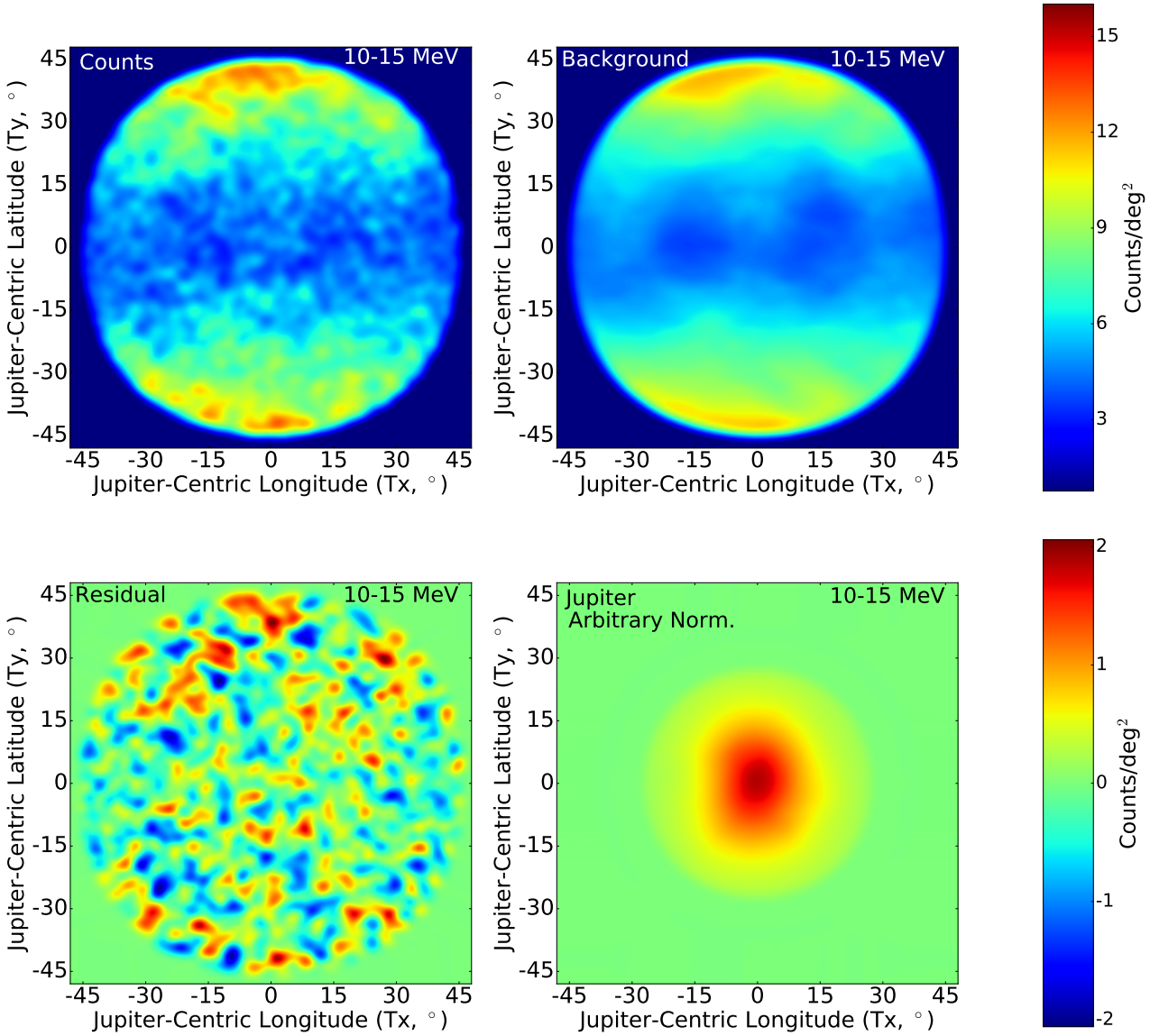

FIG. 3. Same as Figure 2, except for the energy range between 10–15 MeV, where the *Fermi* effective area is small and the angular resolution of the instrument is relatively poor. Results are instead smeared with a 3° Gaussian due to the low photon counts. No obvious errors in the background model appear even at these very low energies. The aspherical appearance of Jupiter is due to ROI cuts from masked sources, which are asymmetric in the Jovian coordinate system.

excess in the lowest energy bins (below 15 MeV). The significance of this excess is 4.6σ in the energy bin between 10—11.2 MeV, 2.3σ in the bin between 11.2—12.6 MeV, and 1.32σ in the bin between 12.6—14.1 MeV. This is a potentially exciting result, pointing to the possibility that Jupiter may be capable of accelerating cosmic-rays to MeV-energies in its strong electromagnetic fields. However, significant caution is warranted for two reasons:

- This analysis severely pushes the limits of the *Fermi*-LAT. To our knowledge, no other study of steady-state emission has taken place in such a low-energy regime. Numerous systematic effects may be present in the low-energy bins that would be difficult to control in any analysis, and a detailed study systematics in this region (which lies beyond the scope of this paper), would be necessary.

- The *Fermi*-LAT effective area rises rapidly with energy in this regime. The exposure at 20 MeV is 50 times larger than at 10 MeV. The fact that no excess is observed in the 20 MeV energy bins strongly constrains the spectrum of any 10 MeV excess. Effectively, any power-law emission at 10 MeV (with spectra harder than $\sim E^{-3}$) is ruled out, and the emission observed at 10 MeV must have a spectrum that is strongly exponentially suppressed.

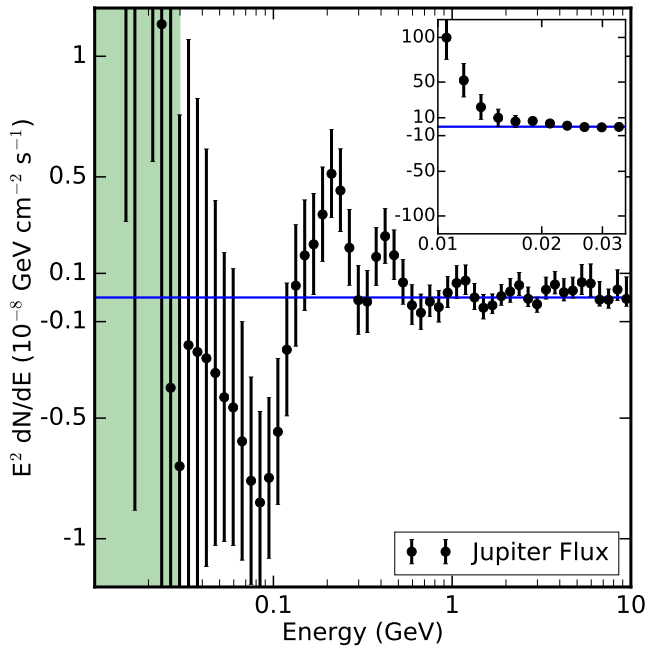

FIG. 4. The gamma-ray flux from Jupiter obtained in our analysis. The blue horizontal line depicts no gamma-ray flux. The significant energy dispersion (especially at low-energies) makes the flux in nearby energy bins highly correlated. Through most of the energy range, we find no evidence for Jovian gamma-ray emission. In the inset (green region), we zoom to show the bright emission in the lowest energy bins. This is potentially statistically significant ($\gtrsim 5\sigma$ when summed over several bins), but occurs below 15 MeV, where *Fermi*-LAT systematic uncertainties are extreme.

However, at present, our analysis can not rule out such a scenario — and we look forward to future observations with MeV-scale gamma-ray missions, such as AMEGO [6] or e-ASTROGAM [7], which could definitively detect, or rule out, this signal. If this emission continues to lower energies, INTEGRAL observations may also be enlightening.

III. DARK MATTER IN JUPITER

In this section, we consider the dynamics of DM in Jupiter, and how a sector with DM and long-lived particles can produce a detectable gamma-ray signal.

A. Dark Matter Capture

DM from the Galactic halo can fall into Jupiter, scattering and losing energy. Once the kinetic energy of the DM is less than the gravitational potential, the DM particle is captured. DM capture can occur via single or multiple scatters with Jovian matter [57, 106–108]. The DM capture rate for N required scatters is given by [106]

$$C_N = \pi R_{♃}^2 p_N(\tau) \frac{\sqrt{6} n_\chi}{3\sqrt{\pi}\bar{v}} \times \left((2\bar{v}^2 + 3v_{\rm esc}^2) - (2\bar{v}^2 + 3v_N^2) \exp\left(-\frac{3(v_N^2 - v_{\rm esc}^2)}{2\bar{v}^2} \right) \right), \quad (1)$$

where $v_{\rm esc} = \sqrt{2\,G\,M_{♃}/R_{♃}} \sim 60\,{\rm km/s}$ is Jupiter's escape velocity with G as the gravitational constant, $M_{♃} = 1.9 \times 10^{27}$ kg and $R_{♃} = 69,911$ km are the mass and radius of Jupiter respectively. $\bar{v}$ is the DM velocity dispersion, $n_\chi(r)$ is the DM number density at the Jupiter position, related to the mass density via $n_\chi(r) = \rho(r)/m_\chi$, and $v_N = v_{\rm esc}(1 - \beta_+/2)^{-N/2}$ with $\beta_+ = 4m_\chi m_n/(m_\chi + m_n)^2$ which takes into account the increasing energy loss with each scatter.

The probability of a single DM particle undergoing N scatters is

$$p_N(\tau) = 2\int_0^1 dy \frac{y e^{-y\tau}(y\tau)^N}{N!}, \quad (2)$$

where τ is the optical depth,

$$\tau = \frac{3}{2}\frac{\sigma}{\sigma_{\rm sat}}, \quad (3)$$

and $\sigma_{\rm sat}$ is the saturation cross section of dark matter capture onto nucleons given by $\sigma_{\rm sat} = \pi R^2/N_n$, where N_n is the number of Jovian nucleons. We assume that Jupiter is a hydrogen sphere (i.e. protons, see subsection below for profile discussion), and conservatively neglect enhancements from molecular hydrogen. The total capture rate of DM in Jupiter $C_{♃}$ is then given by

$$C_{♃} = \sum_{N=1}^{\infty} C_N. \quad (4)$$

We truncate this sum once additional scatters do not change the result more than at about a percent level.

B. Dark Matter Evaporation

The successful capture of DM by Jupiter requires balancing the kinetic energy transferred to the DM from the Jovian core and the gravitational potential energy within Jupiter. As an estimate for the DM evaporation mass, for DM to remain captured and not evaporate, we require

$$\frac{3}{2}T(r) < \frac{GM(r)m_\chi}{2r}, \quad (5)$$

where r is the radius within Jupiter, $M(r)$ is the enclosed Jovian mass at that radius, $T(r)$ is the Jovian temperature as a function of r, and G is the gravitational constant. Eq. 5 shows that as the DM mass decreases, the gravitational potential also decreases and the effects of a thermal kick increase, until the DM particles are no longer retained.

Following Ref. [76], to approximate the DM evaporation mass in Jupiter, we consider two different Jovian density profiles, one with and without a core, from Ref. [109]. This setup features a core temperature of $T_c = 1.5 \times 10^4\,\mathrm{K}$, an average density of $\rho_{♃} = 1.3\,\mathrm{g/cm^3}$, and a radius of $R_{♃} = 6.99 \times 10^7\,\mathrm{m}$. Using Eq. 5, we find that the DM evaporation mass in Jupiter is about 30 MeV independent of our core model. We expect that DM particles with masses approximately larger than this can be captured and subsequently contribute to an annihilation signal.

However, we emphasize that this is not a robust generic calculation of the evaporation mass, and it should instead be taken as an estimate. A few factors can change the evaporation mass. Firstly, while we have considered two different Jupiter profiles here, generally, Jupiter's interior is not robustly known, see e.g. Ref. [110]. Compared to the evaporation value, the interior profile does not as strongly affect the cross section results, as in that case, the total volume the DM particles traverse is more important, rather than the specific distribution of the interior matter. Secondly, our estimate does not take into account the fact that the high energy tail of the thermal Boltzmann distribution can drive evaporation near the evaporation mass. Therefore, we expect a more detailed treatment of the evaporation mass can produce different results, especially in the context of particular particle models. As the goal of our work is to demonstrate the strong power of Jovian gamma rays to probe DM rather than perform a DM model-dependent study, we leave a detailed study of the evaporation mass of Jupiter to future work.

C. Dark Matter Annihilation

If DM can self-annihilate, there is an interplay between the capture and annihilation in Jupiter. DM annihilation depletes the incoming captured DM, such that the number of DM particles inside Jupiter $N(t)$ evolves over time, governed by [57]

$$\frac{dN(t)}{dt} = C_{♃} - C_A N(t)^2 \tag{6}$$

where $C_{♃}$ is the total capture rate given in Eq. 4 and $C_A = \langle \sigma_A v \rangle / V$ is the thermally averaged annihilation cross section over the effective annihilation volume. Eq. 6 has the solution

$$N(t) = \sqrt{\frac{C_{♃}}{C_A}} \tanh \frac{t}{t_{\mathrm{eq}}}, \tag{7}$$

where $t_{\mathrm{eq}} = 1/\sqrt{C_A C_{♃}}$ is the timescale to obtain an equilibrium between capture and annihilation of DM within Jupiter. Once equilibrium has been reached, the annihilation rate (Γ_{ann}) is simply

$$\Gamma_{\mathrm{ann}} = \frac{C_{♃}}{2}, \tag{8}$$

where the factor 1/2 arises because DM annihilation involves two particles. For models with very small capture rates, equilibrium may not be reached within Jupiter's lifetime. However, detectable fluxes are still possible. In this case, the annihilation rate at time t is

$$\Gamma_{\mathrm{ann}}(t) = \frac{N(t)^2}{4\,V_{\mathrm{eff}}} \langle \sigma\, v \rangle, \tag{9}$$

where $\langle \sigma\, v \rangle$ is the thermally averaged DM annihilation cross section, $N(t)$ is the DM number from Eq. 7, $V_{\mathrm{eff}} =$ is the effective volume of DM particles in Jupiter. This assumes non-self-conjugate particles; an additional factor of 2 is required on the right-hand side for self-conjugate particles.

D. Long-Lived Mediator Flux

To provide sensitivities for possible signals, we assume that the mediator ϕ has a sufficiently long lifetime τ or a sufficiently large boost factor $\gamma \approx m_\chi/m_\phi$ such that the decay length L exceeds the radius of Jupiter $R_{♃}$, as

$$L = \gamma\beta\tau \simeq \gamma c\tau > R_{♃}, \tag{10}$$

such that we require

$$\left(\frac{\Gamma_\phi}{\mathrm{GeV}}\right)\left(\frac{m_\phi}{m_\chi}\right) \lesssim 2.9 \times 10^{-24}, \tag{11}$$

where m_χ/m_ϕ is the boost of ϕ in the Jupiter frame, and $\Gamma_\phi = 1/\tau$ is the width of ϕ. The total flux at Earth from long-lived particles in Jupiter is given by [60]

$$E^2 \frac{d\Phi}{dE} = \frac{\Gamma_{\mathrm{ann}}}{4\pi D_\oplus^2} \times E_\gamma^2 \frac{dN_\gamma}{dE_\gamma} \times \mathrm{BR}(\mathrm{X} \to \mathrm{SM}) \times P_{\mathrm{surv}}, \tag{12}$$

where $D_\oplus$ is the average distance of Jupiter to Earth, $\mathrm{BR}(\mathrm{X} \to \mathrm{SM})$ is the branching ratio of the mediator to a given SM final state. The probability of the signal surviving to reach the detector near Earth, P_{surv}, provided the decay products escape Jupiter is [60]

$$P_{\mathrm{surv}} = e^{-R_{♃}/\gamma c\tau} - e^{-D_\oplus/\gamma c\tau}. \tag{13}$$

We assume that the mediator escapes the object without attenuation. This assumption is justified, as long-lived particles generally have weak couplings, which can suppress any scattering cross section of the particle (see Ref. [47] for discussion of this point).

In Eq. 12, the $E_\gamma^2\, dN_\gamma/dE_\gamma$ term corresponds to the gamma-ray energy spectrum. The relevant DM annihilation process is $\chi\overline{\chi} \to \phi\phi \to 4\,\mathrm{SM}$. DM annihilation to two mediators is dominant over DM annihilation to one mediator, as it is not phase-space suppressed. This yields the characteristic gamma-ray box spectral shape [111],

$$\frac{dN_\gamma}{dE_\gamma} = \frac{4}{\Delta E}\Theta(E - E_-)\Theta(E_+ - E), \tag{14}$$

where Θ is the Heaviside function,

$$\Delta E = E_+ - E_- = \sqrt{m_\chi^2 - m_\phi^2} \tag{15}$$

is the spectral box width, and the box edges are

$$E_\pm = \frac{m_\chi}{2}\left(1 \pm \sqrt{1 - \frac{m_\phi^2}{m_\chi^2}}\right). \tag{16}$$

As we consider mediators at least a factor few lighter than the DM, the highest energy gamma rays always peak close to the DM mass. This means that our results are approximately independent of the mediator mass (provided it is sufficiently boosted/long-lived to escape Jupiter).

IV. DARK MATTER RESULTS AND DISCUSSION

Figure 5 shows our new cross section constraints on DM annihilation to long-lived particles using Jovian gamma rays at 95% C.L., for mediator decay to gamma rays, via $\chi\chi \to \phi\phi$, $\phi \to 2\,\gamma$. For definiteness, in this plot we take the mediator to decay at the Jovian surface. We show for comparison, limits from direct detection [112–115], and complementary searches for DM and long-lived particles in the Sun [60, 62], and the Galactic Center population of brown dwarfs [47].

We now discuss how these results compare to other searches, equilibrium assumptions for these results, what can be done with upcoming MeV telescopes, and particle model interpretations.

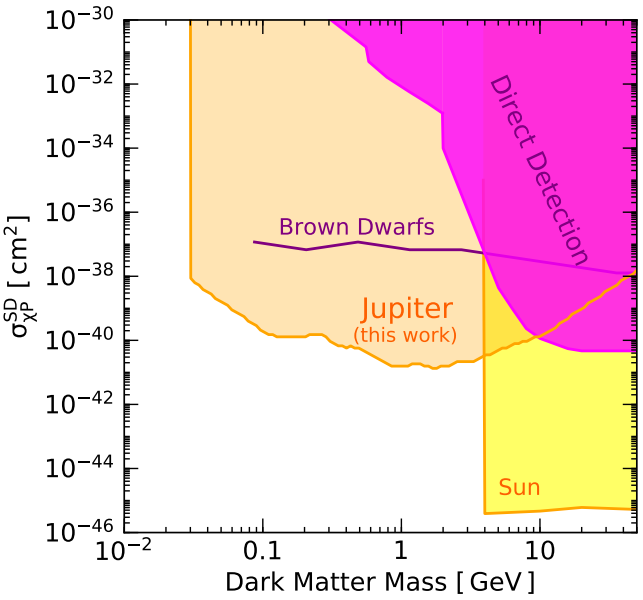

FIG. 5. 95% C.L. DM-proton scattering cross section limits as a function of DM mass m_χ, arising from DM annihilation to long-lived particles, from our new Jovian gamma-ray search. We show complementary constraints from direct detection [112–115], as well as DM annihilation to long-lived particles in the Sun [60, 62], and brown dwarfs in the Galactic center [47]; see text for details.

A. Comparison with Other Searches

In models including DM annihilation to long-lived mediators, searches for Jovian gamma rays provide a superior reach to direct detection searches. In the sub-GeV DM regime, direct detection experiments lose sensitivity as the recoils become increasingly weak, and are eventually below detector thresholds. Jupiter on the other hand, is optimized to search for DM particles with masses of around the proton mass, and has strong sub-GeV DM sensitivity. Note that compared to the Jupiter limits, the direct detection limits do not require any minimum annihilation cross section.

Searches for DM annihilation to long-lived particles in the Galactic Center from a population of brown dwarfs [47] have the most overlap with our new Jovian parameter space. Brown dwarfs in the Galactic bulge are generally old ($\gtrsim$ Gyr), such that their radii are comparable to that of Jupiter (brown dwarfs cool over time, eventually settling into this common radius). Their capture radius is, however, enhanced by the fact that they are more massive, and benefit from gravitational focusing. A large population of brown dwarfs exist in the Galactic center, where they also benefit from large DM densities compared to the local position. However, despite these many benefits, the Galactic center signal is much weaker due to its large distance, with the expected flux diminishing proportionally to the inverse square of the distance. Jupiter on the other hand, is only one object in a comparably low DM density, but it is very close to Earth. This is the main reason the new Jovian search sensitivities are strong in comparison. Note however that brown dwarfs can reach equilibrium for smaller annihilation cross sections than Jupiter (see equilibrium subsection below).

Another nearby, and even bigger object, is the Sun. In Fig. 5 we show limits from DM annihilating to long-lived mediators in the Sun, as calculated in Refs. [60, 62]. We see that the solar limits extend to much lower cross sections, owing to the Sun being much larger than Jupiter and closer to the Earth. However, the Jupiter limits extend to lower DM masses, because Jupiter's cooler core temperature in part can prevent evaporation of sub-GeV DM.

We note that these indirect detection targets are also optimized for different decay lifetimes/boosts of the mediator. The Solar DM search is not sensitive to as short decay lifetimes/as small boosts as Jupiter, as the Sun is an order of magnitude larger in radius, and the particles must therefore travel further to escape the Sun. The GC brown dwarf search has comparable decay lifetime requirements as Jupiter, but has the advantage of probing a wider range of decay lengths; very *long* decay lengths are still likely to be detectable as there is a large

distance between the GC and the *Fermi* Telescope at the local position (see the model subsection for more discussion of model-dependence and interplay of the different constraints in Fig. 5).

A second important difference between the brown dwarf GC limits and Jovian limits, is that the GC limits are highly sensitive to the DM density profile. The brown dwarf limits [47] shown in Fig. 5 are for a Navarro-Frenk-White (NFW) density profile [116], with an inner slope index of $\gamma = 1$. However, it is not currently known if the inner Galaxy exhibits a DM cusp (NFW-like) or core at its center. In this sense, the Jupiter limits are more robust, as the DM density at the solar system position is known to much higher precision. If a cored-DM density profile were the true DM profile, the brown dwarf GC limits would substantially weaken, to be much weaker than our new Jovian constraints. As such, we only show a line for the BD limits; if a NFW profile were observed, cross-sections above this line would be ruled out. If a cored DM density profile were realized, the limits would be much weaker than the line shown.

Finally, we note that we have calculated our Jovian DM limits to 95% C.L., while the solar and brown dwarf limits take a more conservative approach of requiring the DM flux to exceed the measured flux in any energy bin before any limits are set. The Jovian DM limits extend to lower DM masses than those from Galactic center brown dwarfs, despite the higher evaporation mass of DM in Jupiter (for dwarfs, it is estimated to be as low as a few MeV). This is simply because the Galactic center gamma-ray dataset had not been analyzed to as low energies as our Jovian gamma-ray analysis. If they had been, the brown dwarf limits would be expected to extend to lower DM masses than those with Jupiter.

B. Equilibrium Assumptions

We provide some brief estimates on the range of cross sections in Fig. 5 which can lead to equilibrium between DM scattering and annihilation in Jupiter. We find that DM in Jupiter reaches equilibrium for thermally averaged annihilation cross sections of $\langle \sigma_{\rm ann} v_{\rm rel} \rangle \gtrsim 10^{-30} \, (m_\chi/{\rm GeV})^{-1} \, {\rm cm}^3/{\rm s}$, when DM has its geometric scattering cross section in Jupiter of $\sim 10^{-32} \, {\rm cm}^2$. Therefore, for $s-$wave annihilation cross sections to come into equilibrium (which have $\langle \sigma_{\rm ann} v_{\rm rel} \rangle \sim 10^{-26} \, {\rm cm}^3/{\rm s}$), only scattering rates larger than about $\sim 10^{-36} \, {\rm cm}^2$ will come into equilibrium within the current age of Jupiter (4.5 billion years). However, in our estimates here, we very conservatively assumed that the effective annihilation volume is equal to the volume of Jupiter. We emphasize that the equilibration timescale will be much faster if DM thermalizes within Jupiter and settles into a smaller thermal volume, which generically will be true. In this case, lower cross sections can still fall into equilibrium. Thus, in Fig. 5 we show the full potential range that can be probed with Jupiter. Note that even if equilibrium is not reached, a detectable gamma-ray signal can still be produced. In general, the exact limits and thermalization process will depend on the particle DM model in question.

C. Spectra and Upcoming MeV Telescopes

In Fig. 5, we have only shown direct decay to gamma rays $\chi\chi \to \phi\phi \to 4\gamma$ (which is the same as the solar and brown dwarf limits shown). This direct decay to gamma rays is the most optimistic case, providing the strongest limits. However, other final states can also be probed. For example, with electron final states, the DM mass sensitivity can also be extended beyond current solar limits. However, in this case, the increased reach in DM mass will only be a factor of a few, because the electron gamma-ray spectrum is very soft, such that the gamma-ray flux peaks at much lower energies, where the sensitivity is worse. We note that in general, the *Fermi* Telescope's performance is increasingly poor at sub-GeV gamma-ray energies. As such, upcoming MeV telescopes such as AMEGO [6] and e-ASTROGAM [7] may provide more insightful measurements for this lower DM mass range in the near future.

D. Model Interpretation of Results

We have presented our limits in a model-independent way, requiring only that the mediator is sufficiently boosted or long-lived to escape Jupiter. Our goal is not to perform an extensive study of the model possibilities, but rather to point out the strong potential constraining power for DM annihilation to long-lived particles in Jupiter. Given the vast improvement in parameter space from other experiments, we expect a broad range of models can accessed with this new Jovian gamma-ray search. We emphasize that, in terms of limits, we show the optimal scenario. Indeed, depending on the particular model realizations and parameters, these limits can be weaker.

We note, in any case, that a number of models are promising for this region of parameter space. In particular, those already pointed out for DM annihilation to long-lived particles in the Sun can produce similar signals, such as a mixed scalar-pseudoscalar mediator model [61], pseudoscalars [48], vectors or dark Higgs bosons [48]. For example, for the scalar-pseudoscalar model, we expect combinations of DM-mediator couplings of $\lesssim 1$ and proton-mediator couplings $\lesssim 10^{-3}$, mediator less than about an order of magnitude smaller than the given DM mass, can accommodate our Jovian signal (see Ref. [61] for details).

Overall, it is important to keep in mind that the limits shown in Fig. 5 have different assumptions, and in a model-dependent context, the interplay of these bounds will vary. For example, while the limits in Fig. 5 are focused on the sub-GeV mass regime, it is possible that

Jupiter can also be used as a superior target in the GeV and above DM mass range. This can occur, for example, if the decay length is shorter than the Sun radius, such that the solar signal is sufficiently extinguished, leaving weaker or no solar constraints in this higher mass region.

Furthermore, the direct detection constraints may be weakened for classes of models such as inelastic DM, where there are two dark sector states with a mass splitting. The mass splitting can make the up-scatter process of the lighter to the heavier state highly energetically suppressed for direct detection. However, for Jupiter, as it is a different system with different kinematics, it may be possible to still have capture, and a consequent annihilation signal. It is also possible to have more than one mediator present (and can for example be required to provide dark sector mass generation), which also would change the relative phenomenology [117–123].

Lastly, we note that strongly-interacting DM models naturally reside in the sub-GeV parameter space relevant for Jupiter, particularly for the large cross sections that can be probed. This includes Strongly Interacting Massive Particles (SIMPs) [124] and Co-SIMPs [125]. They also are not constrained by any other observations in the relevant parameter space, including indirect detection and direct detection experiments [125]. However, as these classes of models have $3 \to 2$ DM annihilation processes, the gamma-ray energy spectrum will be different to the $2 \to 2$ annihilation assumption used to calculate limits in this work.

V. SUMMARY AND CONCLUSIONS

We searched for King Jupiter's lightning bolts for the first time. Scientifically speaking, we studied Jupiter in gamma rays for the first time, using 12 years of data from the *Fermi* Gamma-Ray Space Telescope. Across most of the gamma-ray energies, we found no gamma-ray flux in excess of background expectations. We therefore set the first upper limits on the Jovian gamma-ray flux.

At lower gamma-ray energies, around tens of MeV, we found a 5σ Jovian gamma-ray excess. However, we emphasize that this excess appears in a region where *Fermi* has very poor angular resolution, energy dispersion, and effective area. Thus, while this excess is interesting, the result should not be taken to be robust. However, this tentative signal motivates follow-up studies with MeV telescopes such as AMEGO or e-ASTROGAM.

We pointed out that Jupiter is an ideal dark matter detector. Compared to the nearby Sun, Jupiter has a cooler core, which can prevent the evaporation of lighter DM particles, allowing new sensitivity to sub-GeV DM. Compared to other solar system planets, Jupiter is much larger, allowing a larger capture and consequent annihilation rate. DM can scatter, become gravitationally captured, and annihilate within Jupiter. If DM annihilates to sufficiently long-lived/boosted mediators, the mediators can escape the Jovian surface, and decay into gamma rays that are detectable by the *Fermi* Telescope. We therefore used our new upper limits on the Jovian flux to constrain, for the first time, the annihilation of DM to long-lived mediators in Jupiter, for DM with masses above about 30 MeV, with DM-proton scattering cross sections down to about $10^{-41}\,\mathrm{cm}^{-1}$. We emphasize, however, that the lower end of the DM mass sensitivity can weaken in some circumstances, due to uncertainties in Jupiter's interior, and in the context of specific particle-model scenarios. Furthermore, we emphasize that the cross section limits can weaken with specific particle models, especially for those which may not reach equilibrium for such small scattering cross sections. These limits should instead be interpreted as demonstrating the strong constraining power of this search, rather than generic, robust constraints. Our results motivate model-dependent studies of the DM parameter space that can be constrained using Jovian gamma rays.

Our new limits on DM annihilation to long-lived particles in Jupiter are about 10 orders of magnitude stronger than terrestrial experiments, such as direct detection. We showed that our Jovian limits are also complementary to other searches for DM annihilation to long-lived particles in the Sun or a Galactic center population of brown dwarfs. While solar DM limits can be stronger for DM masses of a few GeV, Jupiter has a smaller radius, and so can provide sensitivity to shorter mediator decay lengths. Compared to the Galactic center brown dwarf search, a key advantage in our Jupiter search is that it does not depend on the DM density profile, and instead only relies on the local DM density, which is known to much higher precision. It also does not depend on the spatial distribution of the population of many brown dwarfs.

Finally, we note two excesses that deserve additional attention. First, we find a low-significance excess, best fit by the annihilation of a DM particle of mass 493 MeV into long-lived particles which decay directly into gamma rays. However, the local significance of this excess only slightly exceeds 2σ. Additionally, we find statistically significant evidence for Jovian gamma-ray emission below 15 MeV. While this emission has an extremely soft spectrum and is not well fit by any dark matter model (with masses down to 30 MeV), it may provide significant evidence of primary cosmic-ray acceleration within the Jovian atmosphere. However, this analysis pushes the envelope of *Fermi*-LAT's sensitivity as an MeV gamma-ray detector. We emphasize the need for new, and robust analyses for MeV Jovian gamma rays, which can be provided by proposed MeV telescopes.

ACKNOWLEDGMENTS

We thank John Beacom, Joe Bramante, Regina Caputo, Colleen Kron, Nestor Mirabal, Payel Mukhopadhyay, Annika Peter, Juri Smirnov, Natalia Toro, and Bei Zhou for helpful discussions and comments. RKL is supported in part by the U.S. Department of Energy un-

der Contract DE-AC02-76SF00515. TL is partially supported by the Swedish Research Council under contract 2019-05135, the Swedish National Space Agency under contract 117/19 and the European Research Council under grant 742104. This project made use of computing resources from the Swedish National Infrastructure for Computing (SNIC) under the project No. 2020/5-463 partially funded by the Swedish Research Council through grant agreement no. 2018-05973.

[1] N. Giglietto (Fermi-LAT), (2009), arXiv:0907.0541 [astro-ph.SR].
[2] G. Pizzella, European Physical Journal C **78**, 848 (2018), arXiv:1805.06314 [physics.gen-ph].
[3] D. Seckel, T. Stanev, and T. K. Gaisser, Astrophys. J. **382**, 652 (1991).
[4] T. Linden, B. Zhou, J. F. Beacom, A. H. Peter, K. C. Ng, and Q.-W. Tang, Phys. Rev. Lett. **121**, 131103 (2018), arXiv:1803.05436 [astro-ph.HE].
[5] T. Linden, J. F. Beacom, A. H. Peter, B. J. Buckman, B. Zhou, and G. Zhu, (2020), arXiv:2012.04654 [astro-ph.HE].
[6] R. Caputo *et al.* (AMEGO), (2019), arXiv:1907.07558 [astro-ph.IM].
[7] M. Tavani *et al.* (e-ASTROGAM), JHEAp **19**, 1 (2018), arXiv:1711.01265 [astro-ph.HE].
[8] I. Goldman and S. Nussinov, Phys. Rev. D **40**, 3221 (1989).
[9] A. Gould, B. T. Draine, R. W. Romani, and S. Nussinov, Phys. Lett. B **238**, 337 (1990).
[10] C. Kouvaris, Phys. Rev. D **77**, 023006 (2008), arXiv:0708.2362 [astro-ph].
[11] G. Bertone and M. Fairbairn, Phys. Rev. D **77**, 043515 (2008), arXiv:0709.1485 [astro-ph].
[12] A. de Lavallaz and M. Fairbairn, Phys. Rev. D **81**, 123521 (2010), arXiv:1004.0629 [astro-ph.GA].
[13] C. Kouvaris and P. Tinyakov, Phys. Rev. D **82**, 063531 (2010), arXiv:1004.0586 [astro-ph.GA].
[14] S. D. McDermott, H.-B. Yu, and K. M. Zurek, Phys. Rev. **D85**, 023519 (2012), arXiv:1103.5472 [hep-ph].
[15] C. Kouvaris and P. Tinyakov, Phys. Rev. Lett. **107**, 091301 (2011), arXiv:1104.0382 [astro-ph.CO].
[16] T. Guver, A. E. Erkoca, M. Hall Reno, and I. Sarcevic, JCAP **1405**, 013 (2014), arXiv:1201.2400 [hep-ph].
[17] J. Bramante, K. Fukushima, and J. Kumar, Phys. Rev. **D87**, 055012 (2013), arXiv:1301.0036 [hep-ph].
[18] N. F. Bell, A. Melatos, and K. Petraki, Phys. Rev. **D87**, 123507 (2013), arXiv:1301.6811 [hep-ph].
[19] J. Bramante, K. Fukushima, J. Kumar, and E. Stopnitzky, Phys. Rev. **D89**, 015010 (2014), arXiv:1310.3509 [hep-ph].
[20] B. Bertoni, A. E. Nelson, and S. Reddy, Phys. Rev. D **88**, 123505 (2013), arXiv:1309.1721 [hep-ph].
[21] C. Kouvaris and P. Tinyakov, Phys. Rev. **D83**, 083512 (2011), arXiv:1012.2039 [astro-ph.HE].
[22] M. McCullough and M. Fairbairn, Phys. Rev. D **81**, 083520 (2010), arXiv:1001.2737 [hep-ph].
[23] M. Angeles Perez-Garcia and J. Silk, Phys. Lett. **B744**, 13 (2015), arXiv:1403.6111 [astro-ph.SR].
[24] J. Bramante, Phys. Rev. Lett. **115**, 141301 (2015), arXiv:1505.07464 [hep-ph].
[25] P. W. Graham, S. Rajendran, and J. Varela, Phys. Rev. **D92**, 063007 (2015), arXiv:1505.04444 [hep-ph].
[26] M. Cermeno, M. Perez-Garcia, and J. Silk, Phys. Rev. **D94**, 063001 (2016), arXiv:1607.06815 [astro-ph.HE].
[27] P. W. Graham, R. Janish, V. Narayan, S. Rajendran, and P. Riggins, Phys. Rev. **D98**, 115027 (2018), arXiv:1805.07381 [hep-ph].
[28] J. F. Acevedo and J. Bramante, Phys. Rev. **D100**, 043020 (2019), arXiv:1904.11993 [hep-ph].
[29] R. Janish, V. Narayan, and P. Riggins, Phys. Rev. **D100**, 035008 (2019), arXiv:1905.00395 [hep-ph].
[30] R. Krall and M. Reece, Chin. Phys. **C42**, 043105 (2018), arXiv:1705.04843 [hep-ph].
[31] D. McKeen, A. E. Nelson, S. Reddy, and D. Zhou, Phys. Rev. Lett. **121**, 061802 (2018), arXiv:1802.08244 [hep-ph].
[32] M. Baryakhtar, J. Bramante, S. W. Li, T. Linden, and N. Raj, Phys. Rev. Lett. **119**, 131801 (2017), arXiv:1704.01577 [hep-ph].
[33] N. Raj, P. Tanedo, and H.-B. Yu, Phys. Rev. **D97**, 043006 (2018), arXiv:1707.09442 [hep-ph].
[34] N. F. Bell, G. Busoni, and S. Robles, JCAP **1809**, 018 (2018), arXiv:1807.02840 [hep-ph].
[35] R. Garani, Y. Genolini, and T. Hambye, JCAP **1905**, 035 (2019), arXiv:1812.08773 [hep-ph].
[36] C.-S. Chen and Y.-H. Lin, JHEP **08**, 069 (2018), arXiv:1804.03409 [hep-ph].
[37] B. Dasgupta, A. Gupta, and A. Ray, JCAP **08**, 018 (2019), arXiv:1906.04204 [hep-ph].
[38] K. Hamaguchi, N. Nagata, and K. Yanagi, Phys. Lett. **B795**, 484 (2019), arXiv:1905.02991 [hep-ph].
[39] D. A. Camargo, F. S. Queiroz, and R. Sturani, JCAP **1909**, 051 (2019), arXiv:1901.05474 [hep-ph].
[40] N. F. Bell, G. Busoni, and S. Robles, JCAP **1906**, 054 (2019), arXiv:1904.09803 [hep-ph].
[41] R. Garani and J. Heeck, Phys. Rev. **D100**, 035039 (2019), arXiv:1906.10145 [hep-ph].
[42] J. F. Acevedo, J. Bramante, R. K. Leane, and N. Raj, JCAP **03**, 038 (2020), arXiv:1911.06334 [hep-ph].
[43] A. Joglekar, N. Raj, P. Tanedo, and H.-B. Yu, (2019), arXiv:1911.13293 [hep-ph].
[44] A. Joglekar, N. Raj, P. Tanedo, and H.-B. Yu, (2020), arXiv:2004.09539 [hep-ph].
[45] N. F. Bell, G. Busoni, S. Robles, and M. Virgato, (2020), arXiv:2004.14888 [hep-ph].
[46] B. Dasgupta, A. Gupta, and A. Ray, (2020), arXiv:2006.10773 [hep-ph].
[47] R. K. Leane, T. Linden, P. Mukhopadhyay, and N. Toro, (2021), arXiv:2101.12213 [astro-ph.HE].
[48] B. Batell, M. Pospelov, A. Ritz, and Y. Shang, Phys. Rev. D **81**, 075004 (2010), arXiv:0910.1567 [hep-ph].
[49] M. Pospelov, A. Ritz, and M. B. Voloshin, Phys. Lett. B **662**, 53 (2008), arXiv:0711.4866 [hep-ph].
[50] M. Pospelov and A. Ritz, Phys. Lett. B **671**, 391 (2009), arXiv:0810.1502 [hep-ph].

[51] I. Z. Rothstein, T. Schwetz, and J. Zupan, JCAP **07**, 018 (2009), arXiv:0903.3116 [astro-ph.HE].
[52] F. Chen, J. M. Cline, and A. R. Frey, Phys. Rev. D **80**, 083516 (2009), arXiv:0907.4746 [hep-ph].
[53] P. Schuster, N. Toro, and I. Yavin, Phys. Rev. D **81**, 016002 (2010), arXiv:0910.1602 [hep-ph].
[54] P. Schuster, N. Toro, N. Weiner, and I. Yavin, Phys. Rev. D **82**, 115012 (2010), arXiv:0910.1839 [hep-ph].
[55] N. F. Bell and K. Petraki, Journal of Cosmology and Astroparticle Physics **2011**, 003–003 (2011).
[56] J. L. Feng, J. Smolinsky, and P. Tanedo, Phys. Rev. D **93**, 015014 (2016), [Erratum: Phys.Rev.D 96, 099901 (2017)], arXiv:1509.07525 [hep-ph].
[57] C. Kouvaris and P. Tinyakov, Phys. Rev. D **82**, 063531 (2010), arXiv:1004.0586 [astro-ph.GA].
[58] J. L. Feng, J. Smolinsky, and P. Tanedo, Phys. Rev. D **93**, 115036 (2016), [Erratum: Phys.Rev.D 96, 099903 (2017)], arXiv:1602.01465 [hep-ph].
[59] R. Allahverdi, Y. Gao, B. Knockel, and S. Shalgar, Phys. Rev. D **95**, 075001 (2017), arXiv:1612.03110 [hep-ph].
[60] R. K. Leane, K. C. Y. Ng, and J. F. Beacom, Phys. Rev. D **95**, 123016 (2017), arXiv:1703.04629 [astro-ph.HE].
[61] C. Arina, M. Backović, J. Heisig, and M. Lucente, Phys. Rev. D **96**, 063010 (2017), arXiv:1703.08087 [astro-ph.HE].
[62] A. Albert *et al.* (HAWC), Phys. Rev. **D98**, 123012 (2018), arXiv:1808.05624 [hep-ph].
[63] A. Albert *et al.* (HAWC), Phys. Rev. D **98**, 123011 (2018), arXiv:1808.05620 [astro-ph.HE].
[64] M. U. Nisa, J. F. Beacom, S. Y. BenZvi, R. K. Leane, T. Linden, K. C. Y. Ng, A. H. G. Peter, and B. Zhou, (2019), arXiv:1903.06349 [astro-ph.HE].
[65] C. Niblaeus, A. Beniwal, and J. Edsjo, JCAP **11**, 011 (2019), arXiv:1903.11363 [astro-ph.HE].
[66] A. Cuoco, P. De La Torre Luque, F. Gargano, M. Gustafsson, F. Loparco, M. Mazziotta, and D. Serini, Phys. Rev. D **101**, 022002 (2020), arXiv:1912.09373 [astro-ph.HE].
[67] D. Serini, F. Loparco, and M. N. Mazziotta (Fermi-LAT), PoS **ICRC2019**, 544 (2020).
[68] M. Mazziotta, F. Loparco, D. Serini, A. Cuoco, P. De La Torre Luque, F. Gargano, and M. Gustafsson, Phys. Rev. D **102**, 022003 (2020), arXiv:2006.04114 [astro-ph.HE].
[69] N. F. Bell, J. B. Dent, and I. W. Sanderson, (2021), arXiv:2103.16794 [hep-ph].
[70] G. D. Mack, J. F. Beacom, and G. Bertone, Phys. Rev. D **76**, 043523 (2007), arXiv:0705.4298 [astro-ph].
[71] B. Chauhan and S. Mohanty, Phys. Rev. D **94**, 035024 (2016), arXiv:1603.06350 [hep-ph].
[72] J. Bramante, A. Buchanan, A. Goodman, and E. Lodhi, Phys. Rev. D **101**, 043001 (2020), arXiv:1909.11683 [hep-ph].
[73] S. Mitra, Phys. Rev. D **70**, 103517 (2004), arXiv:astro-ph/0408341.
[74] S. L. Adler, Phys. Lett. B **671**, 203 (2009), arXiv:0808.2823 [astro-ph].
[75] M. Kawasaki, H. Murayama, and T. Yanagida, Prog. Theor. Phys. **87**, 685 (1992).
[76] R. K. Leane and J. Smirnov, (2020), arXiv:2010.00015 [hep-ph].
[77] I. Kobzarev, L. Okun, and I. Pomeranchuk, Sov. J. Nucl. Phys. **3**, 837 (1966).
[78] L. Okun, Sov. Phys. JETP **56**, 502 (1982).
[79] B. Holdom, Phys. Lett. B **166**, 196 (1986).
[80] B. Holdom, Phys. Lett. B **178**, 65 (1986).
[81] S. P. Martin, Adv. Ser. Direct. High Energy Phys. **21**, 1 (2010), arXiv:hep-ph/9709356.
[82] M. Reece and L.-T. Wang, JHEP **07**, 051 (2009), arXiv:0904.1743 [hep-ph].
[83] D. E. Morrissey and A. P. Spray, JHEP **06**, 083 (2014), arXiv:1402.4817 [hep-ph].
[84] G. Aad *et al.* (ATLAS), Phys. Rev. D **92**, 072004 (2015), arXiv:1504.05162 [hep-ex].
[85] A. Burrows and J. M. Lattimer, Astrophys. J. Lett. **318**, L63 (1987).
[86] A. Burrows, M. Ressell, and M. S. Turner, Phys. Rev. D **42**, 3297 (1990).
[87] K. Kainulainen, J. Maalampi, and J. Peltoniemi, Nucl. Phys. B **358**, 435 (1991).
[88] G. Raffelt, *Stars as laboratories for fundamental physics: The astrophysics of neutrinos, axions, and other weakly interacting particles* (1996).
[89] C. Hanhart, D. R. Phillips, S. Reddy, and M. J. Savage, Nucl. Phys. B **595**, 335 (2001), arXiv:nucl-th/0007016.
[90] C. Hanhart, J. A. Pons, D. R. Phillips, and S. Reddy, Phys. Lett. B **509**, 1 (2001), arXiv:astro-ph/0102063.
[91] H. Dreiner, C. Hanhart, U. Langenfeld, and D. R. Phillips, Phys. Rev. D **68**, 055004 (2003), arXiv:hep-ph/0304289.
[92] E. Rrapaj and S. Reddy, Phys. Rev. C **94**, 045805 (2016), arXiv:1511.09136 [nucl-th].
[93] J. H. Chang, R. Essig, and S. D. McDermott, JHEP **01**, 107 (2017), arXiv:1611.03864 [hep-ph].
[94] J. H. Chang, R. Essig, and S. D. McDermott, JHEP **09**, 051 (2018), arXiv:1803.00993 [hep-ph].
[95] J. S. Lee, (2018), arXiv:1808.10136 [hep-ph].
[96] W. DeRocco, P. W. Graham, D. Kasen, G. Marques-Tavares, and S. Rajendran, JHEP **02**, 171 (2019), arXiv:1901.08596 [hep-ph].
[97] W. DeRocco, P. W. Graham, D. Kasen, G. Marques-Tavares, and S. Rajendran, Phys. Rev. D **100**, 075018 (2019), arXiv:1905.09284 [hep-ph].
[98] D. Hooper, R. K. Leane, Y.-D. Tsai, S. Wegsman, and S. J. Witte, JHEP **07**, 163 (2020), arXiv:1912.08821 [hep-ph].
[99] F. Ertas and F. Kahlhoefer, (2020), arXiv:2004.01193 [hep-ph].
[100] D. Croon, G. Elor, R. K. Leane, and S. D. McDermott, (2020), arXiv:2006.13942 [hep-ph].
[101] R. Bollig, W. DeRocco, P. W. Graham, and H.-T. Janka, (2020), arXiv:2005.07141 [hep-ph].
[102] A. A. Abdo *et al.*, ApJ **734**, 116 (2011), arXiv:1104.2093 [astro-ph.HE].
[103] S. Abdollahi *et al.*, ApJ **846**, 34 (2017), arXiv:1612.03165 [astro-ph.HE].
[104] "Fermi-LAT P8R3 Energy Dispersion Documentation," `https://fermi.gsfc.nasa.gov/ssc/data/analysis/documentation/Cicerone/Cicerone_LAT_IRFs/IRF_E_dispersion.html`, accessed: 2020-24-03.
[105] T. Linden, Phys. Rev. D **101**, 043017 (2020), arXiv:1905.11992 [astro-ph.HE].
[106] J. Bramante, A. Delgado, and A. Martin, Phys. Rev. D **96**, 063002 (2017), arXiv:1703.04043 [hep-ph].
[107] B. Dasgupta, A. Gupta, and A. Ray, JCAP **08**, 018 (2019), arXiv:1906.04204 [hep-ph].

[108] C. Ilie, J. Pilawa, and S. Zhang, Phys. Rev. D **102**, 048301 (2020), arXiv:2005.05946 [astro-ph.CO].

[109] D. B. Tilman Spohn and T. V. Johnson, **5** (2014), 10.1016/C2010-0-67309-3.

[110] N. Nettelmann, A. Becker, B. Holst, and R. Redmer, The Astrophysical Journal **750**, 52 (2012).

[111] A. Ibarra, S. Lopez Gehler, and M. Pato, JCAP **07**, 043 (2012), arXiv:1205.0007 [hep-ph].

[112] P. Di Gangi (XENON), Nuovo Cim. C **42**, 76 (2019).

[113] E. Aprile *et al.* (XENON), Phys. Rev. Lett. **122**, 141301 (2019), arXiv:1902.03234 [astro-ph.CO].

[114] E. Aprile *et al.* (XENON), Phys. Rev. Lett. **123**, 241803 (2019), arXiv:1907.12771 [hep-ex].

[115] Z. Z. Liu *et al.* (CDEX), Phys. Rev. Lett. **123**, 161301 (2019), arXiv:1905.00354 [hep-ex].

[116] J. F. Navarro, C. S. Frenk, and S. D. White, Astrophys. J. **462**, 563 (1996), arXiv:astro-ph/9508025.

[117] H. An, M. Pospelov, and J. Pradler, Phys. Rev. Lett. **111**, 041302 (2013), arXiv:1304.3461 [hep-ph].

[118] F. Kahlhoefer, K. Schmidt-Hoberg, T. Schwetz, and S. Vogl, JHEP **02**, 016 (2016), arXiv:1510.02110 [hep-ph].

[119] N. F. Bell, Y. Cai, and R. K. Leane, JCAP **08**, 001 (2016), arXiv:1605.09382 [hep-ph].

[120] N. F. Bell, Y. Cai, and R. K. Leane, JCAP **01**, 039 (2017), arXiv:1610.03063 [hep-ph].

[121] M. Duerr, F. Kahlhoefer, K. Schmidt-Hoberg, T. Schwetz, and S. Vogl, JHEP **09**, 042 (2016), arXiv:1606.07609 [hep-ph].

[122] N. F. Bell, Y. Cai, J. B. Dent, R. K. Leane, and T. J. Weiler, Phys. Rev. **D96**, 023011 (2017), arXiv:1705.01105 [hep-ph].

[123] Y. Cui and F. D'Eramo, Phys. Rev. D **96**, 095006 (2017), arXiv:1705.03897 [hep-ph].

[124] Y. Hochberg, E. Kuflik, T. Volansky, and J. G. Wacker, Phys. Rev. Lett. **113**, 171301 (2014), arXiv:1402.5143 [hep-ph].

[125] J. Smirnov and J. F. Beacom, Phys. Rev. Lett. **125**, 131301 (2020), arXiv:2002.04038 [hep-ph].